Brain Topogr (2013) 26:442–457
DOI 10.1007/s10548-012-0265-7

ORIGINAL PAPER

Coupling Between Resting Cerebral Perfusion and EEG

R. L. O'Gorman · S.-S. Poil · D. Brandeis · P. Klaver · S. Bollmann · C. Ghisleni · R. Lüchinger · E. Martin · A. Shankaranarayanan · D. C. Alsop · L. Michels

Received: 15 June 2012 / Accepted: 25 October 2012 / Published online: 18 November 2012
© Springer Science+Business Media New York 2012

Abstract While several studies have investigated interactions between the electroencephalography (EEG) and functional magnetic resonance imaging BOLD signal fluctuations, less is known about the associations between EEG oscillations and baseline brain haemodynamics, and few studies have examined the link between EEG power outside the alpha band and baseline perfusion. Here we compare whole-brain arterial spin labelling perfusion MRI and EEG in a group of healthy adults ($n = 16$, ten females, median age: 27 years, range 21–48) during an eyes closed rest condition. Correlations emerged between perfusion and global average EEG power in low (delta: 2–4 Hz and theta: 4–7 Hz), middle (alpha: 8–13 Hz), and high (beta: 13–30 Hz and gamma: 30–45 Hz) frequency bands in both cortical and sub-cortical regions. The correlations were predominately positive in middle and high-frequency bands, and negative in delta. In addition, central alpha frequency positively correlated with perfusion in a network of brain regions associated with the modulation of attention and preparedness for external input, and central theta frequency correlated negatively with a widespread network of cortical regions. These results indicate that the coupling between average EEG power/frequency and local cerebral blood flow varies in a frequency specific manner. Our results are consistent with longstanding concepts that

Electronic supplementary material The online version of this article (doi:10.1007/s10548-012-0265-7) contains supplementary material, which is available to authorized users.

R. L. O'Gorman · S.-S. Poil · P. Klaver · S. Bollmann · C. Ghisleni · E. Martin · L. Michels (✉)
Center for MR-Research, University Children's Hospital Zurich, Steinwiesstrasse 75, CH-8032 Zurich, Switzerland
e-mail: lars.michels@usz.ch; lars.michels@kispi.uzh.ch

R. L. O'Gorman · D. Brandeis · P. Klaver · E. Martin
Zurich Center for Integrative Human Physiology, University of Zurich, Zurich, Switzerland

D. Brandeis · R. Lüchinger
Department of Child and Adolescent Psychiatry, University of Zürich, Zurich, Switzerland

D. Brandeis
Department of Child and Adolescent Psychiatry and Psychotherapy, Central Institute of Mental Health, Medical Faculty Mannheim/Heidelberg University, Mannheim, Germany

D. Brandeis · P. Klaver
Neuroscience Center Zurich, University of Zurich and ETH Zurich, Zurich, Switzerland

P. Klaver
Institute of Psychology, Division of Abnormal Psychology and Clinical Intervention, University of Zurich, Zurich, Switzerland

A. Shankaranarayanan
GE Medical Systems, Applied Science Lab, Menlo Park, CA, USA

D. C. Alsop
Department of Radiology, Beth Israel Deaconess Medical Center and Harvard Medical School, Boston, MA, USA

L. Michels
Institute of Neuroradiology, University Hospital of Zurich, Zurich, Switzerland

decreasing EEG frequencies which in general map onto decreasing levels of activation.

Keywords Arterial spin labelling · EEG power · Whole-brain perfusion · Resting state

Abbreviations

ASL	Arterial spin labeling
BA	Brodmann area
BOLD	Blood oxygenation level dependent
EEG	Electroencephalogram
FDG	Fluoro-deoxyglucose
FWE	Family-wise error
fMRI	Functional magnetic resonance imaging
ICA	Independent component analysis
MEG	Magnetoencephalography
MNI	Montreal neurological institute
MRT	Magnetic resonance tomography

Introduction

Physiological brain processes can be investigated by a wide array of neuroimaging tools, such as functional magnetic resonance imaging (fMRI), positron emission tomography (PET), scalp surface electroencephalography (EEG), magnetoencephalography (MEG), and arterial spin labelling (ASL) perfusion MRI. These techniques provide interrelated but complementary physiological information, as the fMRI BOLD (blood oxygen level dependent) signal reflects relative changes in the blood oxygenation level (Ogawa et al. 1993; Buxton et al. 2004; Brown et al. 2007), while ASL and PET provide absolute and reproducible values of brain haemodynamics and metabolism (Bartlett et al. 1988; Jahng et al. 2005), and EEG and MEG describe neural activity in absolute terms such as power of electromagnetic oscillations in specific frequency bands (Niedermeyer and Silva 2005; Buzsaki 2006). Because the cellular mechanism underlying EEG (MEG) signals requires the metabolism of glucose and an abundant supply of oxygen, the measured EEG signal is assumed to be closely related to the underlying spatio-temporal pattern of metabolism in the normal human brain (Ingvar et al. 1976; Nagata 1988; Oakes et al. 2004).

Several studies have investigated interactions between the EEG and fMRI BOLD signal fluctuations during resting states (Goldman et al. 2002; Moosmann et al. 2003; Laufs et al. 2003a, b, 2006; Feige et al. 2005; Goncalves et al. 2006; De Munck et al. 2007, 2008; Ben-Simon et al. 2008; Ritter et al. 2009; Jann et al. 2009; Scheeringa et al. 2011), visuo-auditory stimulation (Eichele et al. 2005; Muthukumaraswamy et al. 2009; Mayhew et al. 2010), development (Lüchinger et al. 2011, 2012), and cognition (Meltzer et al. 2007, 2009; Sammer et al. 2007; Scheeringa et al. 2009; Michels et al. 2010, 2012). One general observation is that trial-by-trial fluctuations of EEG power of theta (4–7 Hz) and alpha (8–13 Hz) oscillations are negatively coupled to the BOLD signal. For higher frequencies, such as beta (13–30 Hz) and gamma (>30 Hz), several studies in humans reported positive as well as negative correlations to the BOLD signal (Laufs et al. 2003b; Ritter et al. 2009; Michels et al. 2010; Scheeringa et al. 2011). Nevertheless, interpretations of fMRI BOLD experiments are typically based on the relative differences in oxygenation associated with fluctuations in neuronal activity, without taking into account the neuronal activity and high energy consumption during the baseline state. This approach is only sensitive to relative increases or decreases in signal, and does not account for the absolute signal level. For cognitive tasks it has been reported that the incremental differences in energy observed between task and baseline are small compared to the larger total baseline energy (Ogawa et al. 1993; Hoge and Pike 2001; Kida et al. 2006). This high baseline energy metabolism maintains the subject in a state in which it is possible to respond to external stimuli (Alkire 2008). Importantly, previous studies have demonstrated prominent mnemonic activity during this resting-state (Binder et al. 1999), together with a considerable overlap of brain regions exhibiting high activity during rest (Fox and Raichle 2007) and activation during mnemonic tasks (Buckner 2004; Kuhl et al. 2007). Hence, an understanding of the physiological features of the high baseline energy seems to be prerequisite to understanding and interpreting the small energy increments evoked by a task. Further, previous work suggests that the regional cerebral blood flow (rCBF) signal may be more localized to the underlying neuronal activity than BOLD signal recordings (Duong et al. 2001; Liu et al. 2011). In addition, MRI-perfusion measurements have been shown to demonstrate decreased inter-subject and session variability compared to the BOLD, possibly reflecting a more direct link to neural activity (Aguirre et al. 2002; Wang et al. 2003; Tjandra et al. 2005). Nevertheless, few studies have investigated associations between EEG oscillations and quantitative markers of baseline brain haemodynamics or metabolism. For example, some studies have investigated the relationship between EEG power variations and baseline human rCBF (Sadato et al. 1998) or cerebral glucose metabolism (GluM) by PET (Larson et al. 1998; Lindgren et al. 1999; Dierks et al. 2000; Danos et al. 2001; Jelic et al. 2002; Oakes et al. 2004; Alper et al. 2006). Most of these studies have focused on the magnitude of alpha oscillations, and reported positive GluM-alpha power coupling, although

some studies reported inverse correlations between GluM and EEG power (Larson et al. 1998).

There is evidence that frequency and power are closely interrelated measures (Klimesch 1999), for instance, when it comes to capturing the spectral shifts from slower to faster frequencies with maturation (Lüchinger et al. 2011, 2012), or with increasing vigilance and activation within and across bands (Buzsaki 2006). A recent study investigating simultaneous resting EEG and ASL found a positive correlation between individuals' central alpha frequency and rCBF, in a network of brain regions associated with the modulation of attention and preparedness for external input (Jann et al. 2010), indicating that not only power but also individuals' central frequency is linked to haemodynamics. However, only few studies have addressed the question of how EEG power and central frequency outside the alpha band are related to baseline metabolic or hemodynamic differences. These studies reported a positive interaction between the index of GluM and beta band (and alpha) power (Dierks et al. 2000) or bidirectional interactions of frequency band power and GluM in healthy subjects (Oakes et al. 2004; Alper et al. 2006). Addressing power fluctuations not only in lower but also in higher frequency bands is important to improve our understanding of physiological brain processes at a broader level, since variations within these frequency bands have been linked to learning (Gruber et al. 2001; Axmacher et al. 2006), memory (Raghavachari et al. 2001; Jensen et al. 2002; Jokisch and Jensen 2007; Tuladhar et al. 2007; Montez et al. 2009), attention (Kranczioch et al. 2006), motor imagination (De Lange et al. 2008), and motor planning (Van der Werf et al. 2008).

In this study we examine the coupling between eyes-closed resting EEG power and central frequency and resting cerebral perfusion using ASL in healthy adults. Based on the existing literature from EEG-fMRI and EEG-ASL resting state studies we hypothesised that low (delta/theta: 1–7 Hz) frequency band power would be predominantly negatively correlated to perfusion, while middle and high frequency band power (alpha/beta/gamma: 8–45 Hz) would be predominantly positively correlated with perfusion. We additionally tried to replicate the previously reported positive coupling between alpha peak frequency and regional perfusion (Jann et al. 2010).

Materials and Methods

Subjects

The subject group consisted of 16 healthy volunteers (ten females, median age: 27 years, range 21–48) with no history of neurological or psychiatric illness, illegal substance abuse or use of psychotropic medication. All subjects refrained from caffeine, alcohol, and nicotine for at least 6 hours before the experiment.

EEG-Data Acquisition

The EEG was recorded outside the MRI scanner using two BrainAmp amplifiers (Brain Products, Munich, Germany) connected to the EEG monitor via optical fibres. The EEG was recorded in DC mode at a resolution of 0.1 μV, with a 250 Hz low-pass filter. A 2.5 min eyes-closed resting-state EEG recording was acquired. Data were sampled at 5,000 Hz with a 3.3 mV input range, and off-line re-sampled to 500 Hz. EEG was recorded from sixty scalp electrode locations. All electrode positions of the 10–20 system plus the following 10–10 system sites were used: Fpz, AFz, FCz, CPz, POz, Oz, Iz, F5/6, FC1/2/3/4/5/6, FT7/8/9/10, C1/2/5/6, CP1/2/3/4/5/6, TP7/8/9/10, P5/6, PO1/2/910, OI1/2. O1/2 and Fp1/2 were placed 2 cm laterally from the standard positions for more even coverage (Halder et al. 2005; Maurer et al. 2007; Brem et al. 2010). F1 served as the recording reference, and F2 served as the ground electrode. Two additional electrodes were placed below the outer canthus of each eye and two further electrodes were positioned adjacent to the sternum and on the left chest close to the heart, to record the electrocardiogram. Electrode impedances were kept below 30 kΩ.

MRI-Data Acquisition

MR imaging studies were performed with a 3.0 T GE HD.xt whole-body MRI scanner (GE Medical Systems, Milwaukee, WI, USA), using an 8-channel receive-only head coil and a body transmit coil. Cerebral perfusion images were collected during a 5 min eyes-closed resting condition with a background-suppressed, pulsed continuous arterial spin labelling (pCASL) sequence, using a 3D stack of spirals fast spin echo readout (Dai et al. 2008). Thirty-two axial slices were collected with a repetition time (TR) of 5.5 s and an echo time (TE) of 25 ms, a slice thickness (ST) of 4 mm, a field of view (FOV) of 24 cm, 3 Nex, and a nominal in-plane resolution of 1.9×1.9 mm^2. A post-labelling delay of 1.5 s was used to reduce errors from transit time effects (Alsop and Detre 1996). Participants were instructed to keep their eyes closed during acquisition of the perfusion images. Structural images were obtained with a 3D T1-weighted gradient echo pulse sequence (number of slices = 172, ST = 2.0 mm, TR = 9.988 ms, TE = 2.916 ms, FOV = 240 mm × 240 mm, flip angle = 20°, matrix = 256 × 192, reconstructed voxel resolution: 0.8 × 0.8 × 1.2 mm). The head was immobilized using foam pads and participants were provided with earplugs. The EEG and ASL perfusion

measurements were performed consecutively in the same measurement session, with an intervening time gap of approximately 30 min.

Data Analysis

EEG Preprocessing

EEG data were processed offline using the Brain Vision Analyzer software (version 1.05, Brain Products, Munich, Germany) and the Neurophysiological Biomarker Toolbox (http://www.nbtwiki.net/). ECG channels were discarded from further analysis. Major transient artifacts such as large muscle or motion artifacts (typical duration: 2.5 s, range 0.4–32.6 s) were removed from the EEG before ICA. Data was digitally high-pass filtered for ICA cleaning (0.5 Hz, finite impulse response filter, 4 s Hanning window), and rank reduced using PCA to cover 97.5 % of the explained variance. An extended ICA (Delorme and Makeig 2004) was calculated to decompose the measured signal into EEG and artefact components (Jung et al. 2000a, b). Components clearly assigned to either eye blink or muscle artefacts were excluded from the back projection. The EEG was then transformed to the average reference (Lehmann and Skrandies 1980). The power spectral density was estimated using Bartlett's method, whereby the EEG signal was segmented into windows of 512 points and convolved with a Hamming window. Before FFT the window was zero-padded to 16,384 points to interpolate the FFT resolution from 0.98 to 0.03 Hz. The average band power was calculated as the integrated area under the absolute power spectrum in the specific frequency band of interest, divided by the width (in points) of the specific frequency band. To estimate the total activity over the scalp, global spectral power (GSP) was calculated as the root mean square (RMS) of the power spectral density across all channels (Jann et al. 2009; Michels et al. 2010). GSP was selected because it summarizes EEG activity across channels and represents spectral activity without preselected electrodes, topographic components, or sources. We additionally performed a correlation analysis between perfusion and locally-restricted alpha EEG power and central frequency values in left and right hemispheres (excluding mid-line electrodes), and the O2 channel. The central frequency was calculated as:

$$CF = \frac{\sum fP(f)}{\sum P(f)},$$

according to the method described (Jann et al. 2010; Vural and Yildiz 2010). EEG-ASL correlations were calculated for power and central frequency in the delta (1–4 Hz), theta (4–7 Hz), alpha (8–13 Hz), beta (13–30 Hz), and gamma (30–45 Hz) bands.

MRI Preprocessing

The perfusion images were quantified using the model proposed by (Alsop and Detre 1996), with additional terms included to represent the finite labelling duration (Wang et al. 2005) and to correct for incomplete recovery of the magnetisation in the reference image due to the saturation applied t_{sat} (2,000 ms) before imaging. The perfusion was calculated according to the following equation (Alsop and Detre 1996; Järnum et al. 2010):

$$f = \frac{\lambda}{2\alpha T_{1b}\left(1 - e^{-\frac{\tau}{T_{1b}}}\right)} \frac{(S_{ctrl} - S_{lbl})\left(1 - e^{-\frac{t_{sat}}{T_{1g}}}\right)}{S_{ref}} e^{\frac{w}{T_{1b}}},$$

where f is the perfusion (in ml/min/100 ml), $S_{ctrl} - S_{lbl}$ is the difference image (control-label), and S_{ref} is a proton-density weighted reference image. λ is the blood brain partition coefficient (0.9), α is the inversion efficiency, T_{1b} is the T_1 of blood (1,600 ms), T_{1g} is the T_1 of grey matter (1,200 ms), w is the post-labelling delay (1.5 s), and τ is the labelling duration (1.5 s). The labelling efficiency is given by the product of the PCASL labelling efficiency (0.95) and an additional efficiency factor which incorporates the loss of efficiency from the background suppression (0.75). This model assumes that the labelled spins remain primarily in the microvasculature rather than exchanging with tissue water, so the T_1 of blood is used for quantification (Wang et al. 2005; Järnum et al. 2010).

A standardised group-specific perfusion template (spatial resolution: $2 \times 2 \times 2$ mm^3) was generated by normalising the perfusion images for each subject to the SPM EPI template using SPM 5 (Wellcome Department of Cognitive Neurology, London, UK; http://www.fil.ion.ucl.ac.uk/spm), and then calculating a mean perfusion image from the normalised perfusion images for each subject. The original (un-registered) perfusion images for each subject were then normalised to the perfusion template using the FLIRT algorithm in FSL, (http://www.fmrib.ox.ac.uk) using the correlation ratio as the cost function (Wastling et al. 2009). The normalised perfusion images were then smoothed in SPM with a four mm Gaussian smoothing kernel.

Statistical Analysis

The relationship between perfusion and maximum GSP was tested for each frequency band separately at the level of voxel clusters by fitting a multiple linear regression model onto the perfusion values at each intracerebral voxel, using the nonparametric permutation-based methods

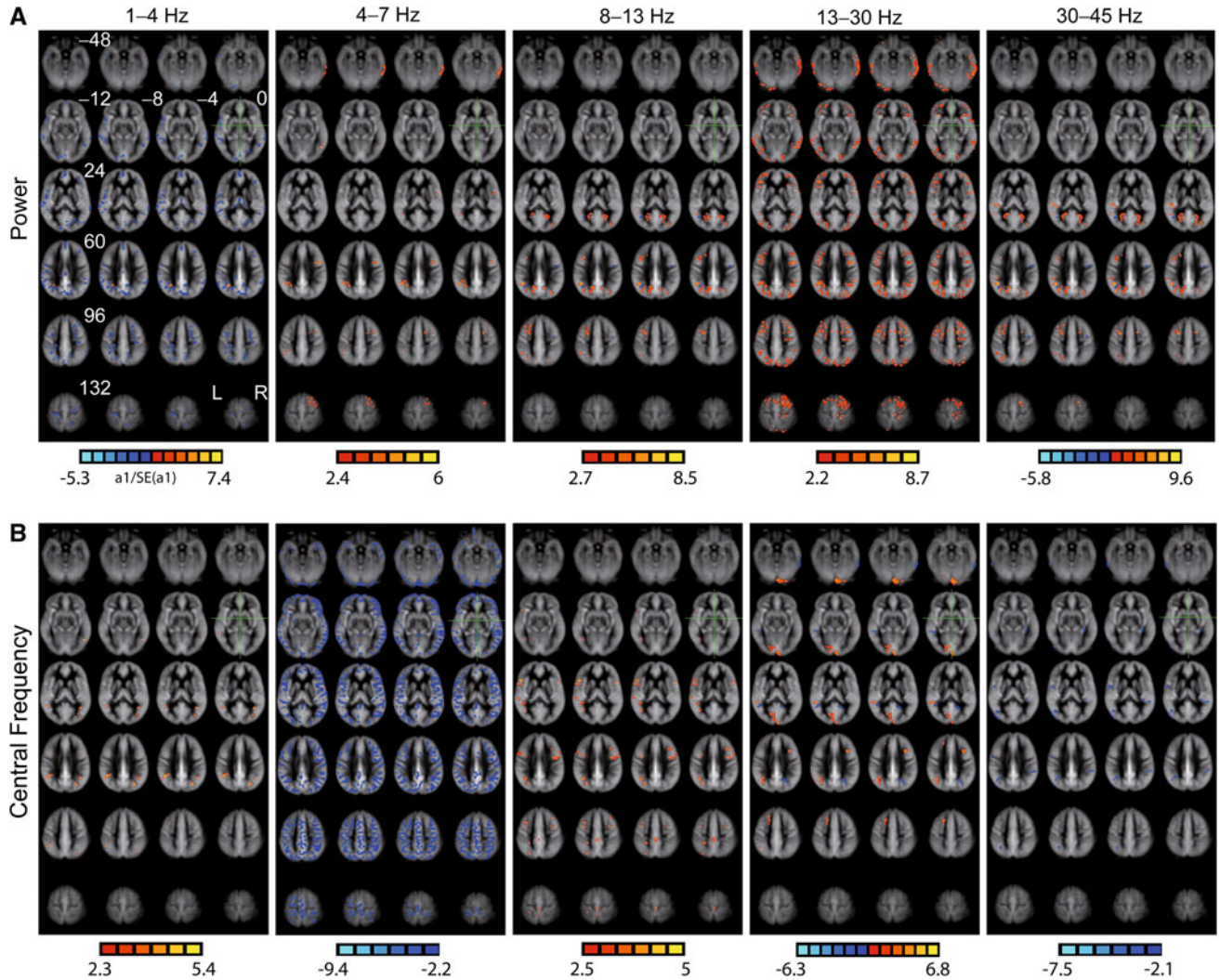

Fig. 1 Resting whole-brain perfusion correlations with eyes-closed EEG power and central frequency. **a** Correlation analysis of ASL perfusion versus EEG power in different frequencies covaried for age and gender. *Blue* indicates negative correlations and *red* indicates positive correlations. The *green* cross indicates the reference point, and *z-coordinates* from this reference point are indicated in first panel, **b** same as in "**a**", but for EEG central frequency. All nonparametric correlations shown here are significant at a threshold of $p < 0.05$ (FWE corrected). The *scale bar* denotes the range of the standardised test statistic from the permutation test (given by the coefficient a1 divided by its standard error) with brighter values indicating increasing significance (Color figure online)

implemented in the Cambridge Brain Analysis (CamBA) software (Suckling and Bullmore 2004; Chamberlain et al. 2009). Age and gender were included as covariates in the regression model.

$$P = a1\ \text{EEG power(frequency)} + a2\ \text{gender} + a3\ \text{age} + e,$$

where P is the perfusion at a particular voxel, $a1$ is the coefficient relating EEG power (or frequency) to perfusion at a particular voxel, $a2$ and $a3$ are the coefficients for the covariates of gender and age, and e is an error term.

This model was regressed repeatedly at each voxel after random permutation of the vector of EEG power and frequency values across the group, and a preliminary null distribution of the signed coefficient $a1$ (standardised by its standard error) was derived by pooling the resulting estimates of $a1$ over all intracerebral voxels. Spatial clusters of significant voxels were defined and the cluster mass statistic was tested against the distribution of cluster mass values derived from the permuted maps. The significance thresholds were corrected for multiple comparisons by controlling the number of error clusters per image and the family-wise error rate (FWE). Results are shown at $p < 0.05$ and brighter colours on the accompanying scale bar (Figs. 1, 2) denote higher significance. To estimate the linear correlation between EEG parameters and perfusion, we additionally calculated Pearson's correlations for selected clusters. All correlations are reported in Talairach space (Talairach and Tournoux 1988).

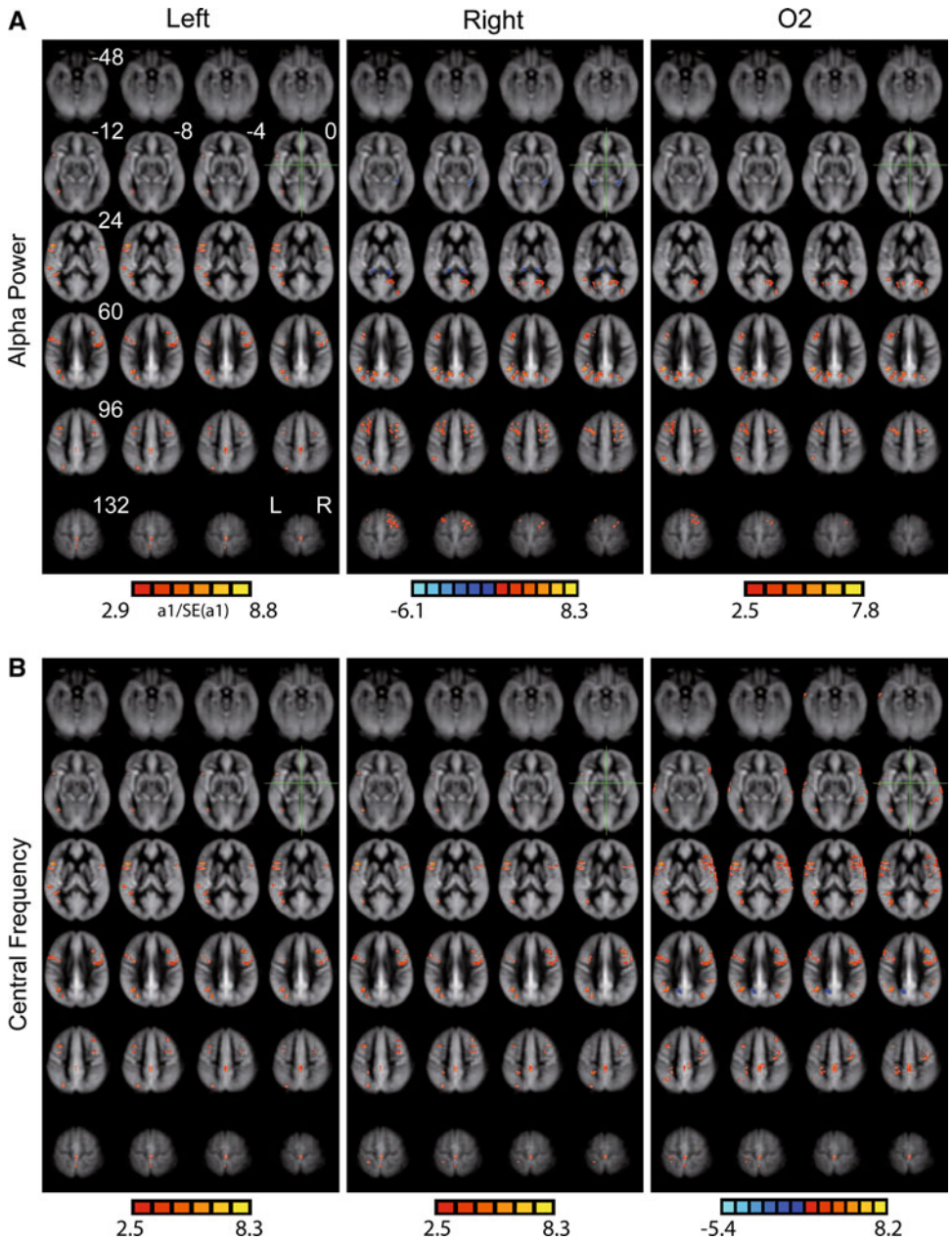

Fig. 2 Resting whole-brain perfusion correlations with locally restricted eyes-closed EEG alpha power and central frequency. **a** Correlation analysis of ASL perfusion versus EEG-power in different frequencies covaried for age and gender from left/right hemisphere (excluding *midline*), and O_2. *Blue* indicates negative correlations and *red* indicates positive correlations. The *green* cross indicates the reference point, and *z-coordinates* from this reference point are indicated in first panel, **b** same as in "**a**", but for EEG central frequency. All nonparametric correlations shown here are significant at a threshold of $p < 0.05$ (FWE corrected) (Color figure online)

Results

The distribution of the absolute spectral EEG power and the topographical maps for the different frequency bands are shown in Fig. 3. Most power was observed in the alpha band, and the topographical maps reveal that power in all frequency bands was strong at parieto-occipital electrodes. Beta and gamma power maps appear uncontaminated by muscle or eye movement artefacts, as spectral power was not prominently enhanced at temporal and frontal electrodes or at the two eye electrodes (Fig. 3).

We observed average power values of: delta (1–4 Hz) 3.2 ± 2.3 μV^2/Hz, theta (4–7 Hz) 1.2 ± 1.7 μV^2/Hz, alpha (8–13 Hz) 5.6 ± 10 μV^2/Hz, beta (13–30 Hz) 0.4 ± 0.2 μV^2/Hz, gamma (30–45 Hz) 0.04 ± 0.03 μV^2/Hz, and central frequencies of: Delta 2.1 ± 0.2 Hz, theta 5.6 ± 0.1 Hz, alpha 10.2 ± 0.4 Hz, beta 19.1 ± 0.6 Hz, and gamma 36.2 ± 0.5 Hz.

The analysis of interactions between average EEG power and pCASL whole-brain perfusion revealed predominantly negative correlations in the delta band and predominantly positive correlations in theta, alpha, beta, and gamma bands (Fig. 1). Correlations were observed in an extensive network of cortical regions, which varied considerably between frequency bands (see Table 1 for Talairach coordinates). Delta power showed predominantly negative correlations in the thalamus and fronto-parietal regions, and theta power showed primarily positive correlations with perfusion in the inferior frontal and temporal gyri, as well as inferior parietal and superior frontal regions. Alpha power was significantly correlated with perfusion in the posterior cingulate gyrus, precuneus, and inferior and medial frontal gyri, while beta power showed positive correlations with perfusion in a widespread network of parietal, frontal, occipital, and temporal regions. Gamma power exhibited mainly positive correlations with perfusion in the posterior cingulate, precuneus, media frontal gyrus and cerebellum.

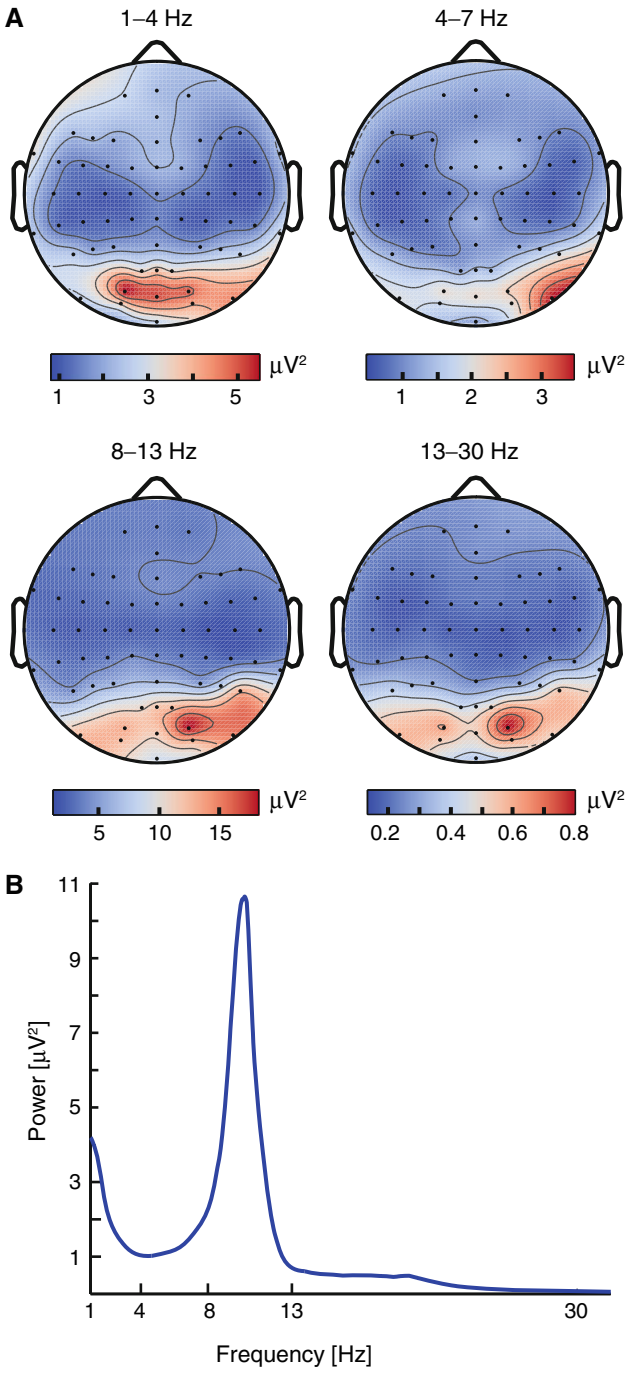

Fig. 3 EEG oscillations during eyes-closed rest. **a** Grand average *topographical plot* of EEG power in specific frequency bands (median across subjects), **b** *power spectral density plot* (Welch's method)

Delta central frequency was positively correlated with perfusion in the middle temporal gyrus and inferior parietal lobule. Central theta frequency showed a strong negative correlation with perfusion in a widespread network of cortical regions, which is also seen in the Pearson's correlations analysis ($p < 0.01$, $r = -0.79$, Supplementary Figure 1; bottom panel). Beta central frequency was positively correlated with perfusion in the lingual gyrus and medial frontal gyrus, but negatively correlated with perfusion in the posterior cingulate and medial temporal gyrus. Central alpha frequency was positively correlated with perfusion in the inferior frontal gyrus, which was also evident from the linear correlation analysis ($p < 0.01$, $r = 0.63$, Supplementary Figure 1; top panel), Central alpha frequency showed additional positive correlations with perfusion in insular cortex and inferior parietal regions. Gamma central frequency demonstrated a negative coupling to perfusion in the middle and inferior temporal gyrus, as well as inferior frontal and parietal regions.

The analysis of average (integrated) alpha power and central frequency for electrode O2 demonstrated a similar pattern to that observed for the GSP (Fig. 2). Correlations between perfusion and alpha frequency calculated for the left and right electrodes separately appeared to be independent of EEG laterality, but the correlations between alpha power and perfusion revealed some differences depending on whether alpha power was calculated from the left or right electrodes or from the GSP ($p < 0.05$, Fig. 2). Specifically, when alpha power was calculated from the right electrodes only, negative correlations emerged between alpha power and perfusion in the posterior thalamus and parahippocampal gyrus in conjunction with positive correlations in the posterior cingulate and medial frontal and occipital gyri. When alpha power was calculated for the left electrodes only, exclusively positive correlations were seen in inferior and medial frontal and occipital regions.

Figure 4 shows perfusion maps for a single subject (top panel) and a group map (bottom panel) derived from the average perfusion across all subjects. High perfusion can

Table 1 List of cluster coordinates for brain regions demonstrating significant ($p < 0.05$, FWE corrected) EEG-ASL correlations with EEG power and frequency in the different frequency bands

Region	Hemisphere	Talairach coordinates	Direction	Brodmann
Delta power				
Gyrus frontalis superior pars medialis	Left	X:−2, Y:55, Z:18	Negative	9
Middle frontal gyrus	Right	X:36, Y:34, Z:24	Negative	46,9
Superior temporal gyrus	Right	X:50, Y:−50, Z:14	Negative	22
Cerebellum	Right	X:50, Y:−75, Z:27	Negative	
Corpus callosum		X:0, Y:−12, Z:23	Negative	
Gyrus frontalis superior	Right	X:22, Y:−8, Z:69	Negative	6
Precuneus, cuneus	Right	X:2, Y:−76, Z:41	Negative	7,17
Gyrus occipitotemporalis medialis	Left	X:−20, Y:−93, Z:−7	Negative	18,17
Cingulate gyrus	Left	X:−18, Y:−39, Z:39	Negative	31
Superior temporal gyrus	Left	X:−50, Y:−40, Z:22	Negative	22
Precentral gyrus	Left	X:−51, Y:−1, Z:13	Negative	4,6
Angular gyrus	Left	X:−32, Y:−54, Z:39	Positive	39
Theta power				
Gyrus frontalis superior pars medialis	Right	X:16, Y:8, Z:47	Positive	6
Inferior frontal gyrus	Right	X:38, Y:7, Z:31	Positive	44
Inferior temporal gyrus	Right	X:59, Y:−54, Z:−9	Positive	37
Inferior parietal lobule	Left	X:−46, Y:−49, Z:34	Positive	40
Superior frontal gyrus	Right	X:24, Y:19, Z:62	Positive	6
Alpha power				
Precuneus	Right	X:20, Y:−63, Z:25	Positive	18
Precentral gyrus	Right	X: 40, Y:−2, Z:35	Positive	6
Middle frontal gyrus	Left	X:−40, Y:13, Z:27	Positive	9
Inferior parietal lobule, angular gyrus	Left	X:−40, Y:−54, Z:40	Positive	39,40
Cingulate gyrus	Left	X:−14, Y:−59, Z:27	Positive	31
Orbital gyri	Right	X:30, Y:−72, Z:31	Negative	19
Inferior frontal gyrus	Right	X:40, Y:−2, Z:33	Negative	9
Middle frontal gyrus	Left	X:−40, Y: 11, Z:34	Negative	9
Inferior parietal lobule, angular gyrus	Left	X:−40, Y:−66, Z:35	Negative	39,40
Beta power				
Middle frontal gyrus	Left	X:−38, Y:21, Z:30	Positive	9
Orbital gyri, angular gyrus	Left	X:−34, Y:−76, Z:31	Positive	19
Superior parietal gyrus	Right	X:31.68, Y:−71.24, Z:51.47	Positive	7
Middle frontal gyrus	Right	X:42, Y:−50, Z:−1	Positive	21
Inferior temporal gyrus, middle gyrus	Right	X:48, Y:−17, Z:−18	Positive	20,21
Paracentral lobule	Right	X:6, Y:−26, Z:58	Positive	6
Middle frontal gyrus	Right	X:28, Y:37, Z:41	Positive	8
Gamma power				
Cerebellum	Left	X:−13, Y:−84, Z:−28	Positive	
Precuneus	Right	X:20, Y:−63, Z:25	Positive	31
Inferior frontal gyrus	Right	X:40, Y:−2, Z:33	Positive	44
Gyrus frontalis superior pars medialis	Right	X:16, Y:8, Z:51	Positive	8
Middle frontal gyrus	Left	X:−28, Y:19, Z:40	Positive	8
Inferior parietal lobule	Left	X:−47, Y:−34, Z:27	Positive	40
Inferior parietal lobule	Left	X:−30, Y:−58, Z:38	Positive	40
Cingulate gyrus	Left	X:−30, Y:−6, Z:42	Negative	24
Cingulate gyrus	Right	X:18, Y:8, Z:46	Negative	32,6
Inferior frontal gyrus	Right	X:40, Y:−2, Z:33	Negative	44

Table 1 continued

Region	Hemisphere	Talairach coordinates	Direction	Brodmann
Precuneus	Right	X:24, Y:−63, Z:35	Negative	7
Inferior parietal lobule, angular gyrus	Left	X:−42, Y:−57, Z:34	Negative	40,39
Central delta frequency				
Inferior parietal lobule	Left	X:−46, Y:−49, Z:26	Positive	40
Middle temporal gyrus	Right	X:38,Y:−54, Z:16	Positive	39
Middle temporal gyrus	Right	X:30, Y:−72, Z:29	Positive	39
Central theta frequency				
Gyrus occipitotemporalis lateralis	Right	X:36, Y: 34, Z:−13	Negative	11,47
Cingulate gyrus	Left	X:−14, Y:−69, Z:12	Negative	23,29,30
Gyrus occipitotemporalis lateralis	Left	X:−38, Y:44, Z:44	Negative	8
Middle temporal gyrus	Right	X:45, Y:55, Z:4	Negative	21,22
Central alpha frequency				
Cerebellum	Left	X:−40, Y:−92, Z:−28	Positive	
Inferior frontal gyrus	Right	X:51, Y:6, Z:33	Positive	44
Inferior frontal gyrus	Left	X:−46, Y:9, Z:29	Positive	44
Inferior parietal lobule	Left	X:−40, Y:−57, Z:25	Positive	39,40
Paracentral lobule	Left	X:−4, Y:−31, Z:49	Positive	4,5
Paracentral lobule	Left	X:−4, Y:−29, Z:51	Positive	5
Central beta frequency				
Inferior frontal gyrus	Right	X:32, Y:17, Z:30	Positive	44
Gyrus frontalis superior	Left	X:−20, Y:20, Z:43	Positive	8
Superior temporal gyrus	Left	X:−46, Y:−46, Z:21	Positive	22
Gyrus occipitotemporalis medialis	Left	X:−6, Y:−78, Z:4	Positive	18
Cerebellum	Left	X:−4, Y:−60, Z:−31	Positive	
Cuneus		X:0, Y:−93, Z:10	Positive	18,17
Gyrus occipitotemporalis lateralis	Right	X:57, Y:−35, Z:−22	Negative	20,36
Superior temporal gyrus	Left	X:−46, Y:−46, Z:21	Negative	22,42
Cerebellum	Left	X:−2, Y:−58, Z:−28	Negative	
Gyrus occipitotemporalis medialis	Left	X:−6, Y:−75, Z:6	Negative	18
Cingulate gyrus	Right	X:18, Y:−57, Z:27	Negative	31
Cingulate gyrus	Right	X:32, Y:17, Z:30	Negative	32
Middle frontal gyrus	Left	X:−24, Y:29, Z:39	Negative	8
Central gamma frequency				
Middle temporal gyrus	Left	X:−46, Y:−63, Z:22	Negative	22
Middle temporal gyrus	Left	X:−63, Y:−58, Z:−1	Negative	37
Inferior frontal gyrus	Left	X:−55, Y:1, Z:17	Negative	44
Transverse temporal gyrus	Right	X:36, Y:−34, Z:15	Negative	41
Inferior parietal lobule	Left	X:−36, Y:−54, Z:45	Negative	40

be observed in the precuneus, insular cortex, posterior cingulate cortex, posterior parietal cortex, cerebellum, brain stem, and prefrontal cortex, including the anterior cingulate cortex.

Discussion

In comparison to previous studies which used either the mean global CBF (Ingvar et al. 1979; Kuschinsky et al. 1993) or specific regions of interests (Alper et al. 2006), our analysis provides a detailed voxel-based analysis of the correlations between average EEG band power, central frequency, and ASL perfusion (Oakes et al. 2004; Jann et al. 2010). Additionally, the present study showcases an approach that permits a global, whole-brain and local (e.g., O2 electrode) correlation analysis of EEG and ASL data. Our main finding was that EEG power correlations with ASL perfusion vary considerably between frequency bands, such that delta oscillations demonstrate negative

correlations between perfusion and EEG power while middle and higher (alpha, beta, and gamma) frequency bands demonstrate positive correlations. Interestingly, the regions demonstrating significant correlations between perfusion and alpha and gamma power appear to overlap. Theta central frequency showed strong negative correlations with perfusion in a widespread network of brain regions, whereas the central frequency in other frequency bands mainly displayed localised positive correlations with perfusion.

Although the neurophysiological basis for the relationship between EEG power and perfusion has not yet been established, the summed excitatory and inhibitory post-synaptic potentials which are thought to account for most of the EEG are the product of modulations of ionic conductance that require metabolic energy (Pilgreen 1995). The first studies examining the link between global CBF and EEG frequency showed a positive correlation between metabolism and electrical activity (Ingvar et al. 1976, 1979; Kuschinsky et al. 1993). On a cellular level, both excitatory and inhibitory signals appear to contribute to an increase in rCBF, not only in the region producing the excitatory/inhibitory signals but additionally in the region receiving them (Mathiesen et al. 1998). Efforts to model the relationship between cellular spiking and synaptic activity and the CBF signal contradict the notion than an excitatory signal is always related to an increase in metabolism, and conversely that inhibitory signals must yield a deactivation (Almeida and Stetter 2002). Ensembles of individual neurons act in synchrony to produce an

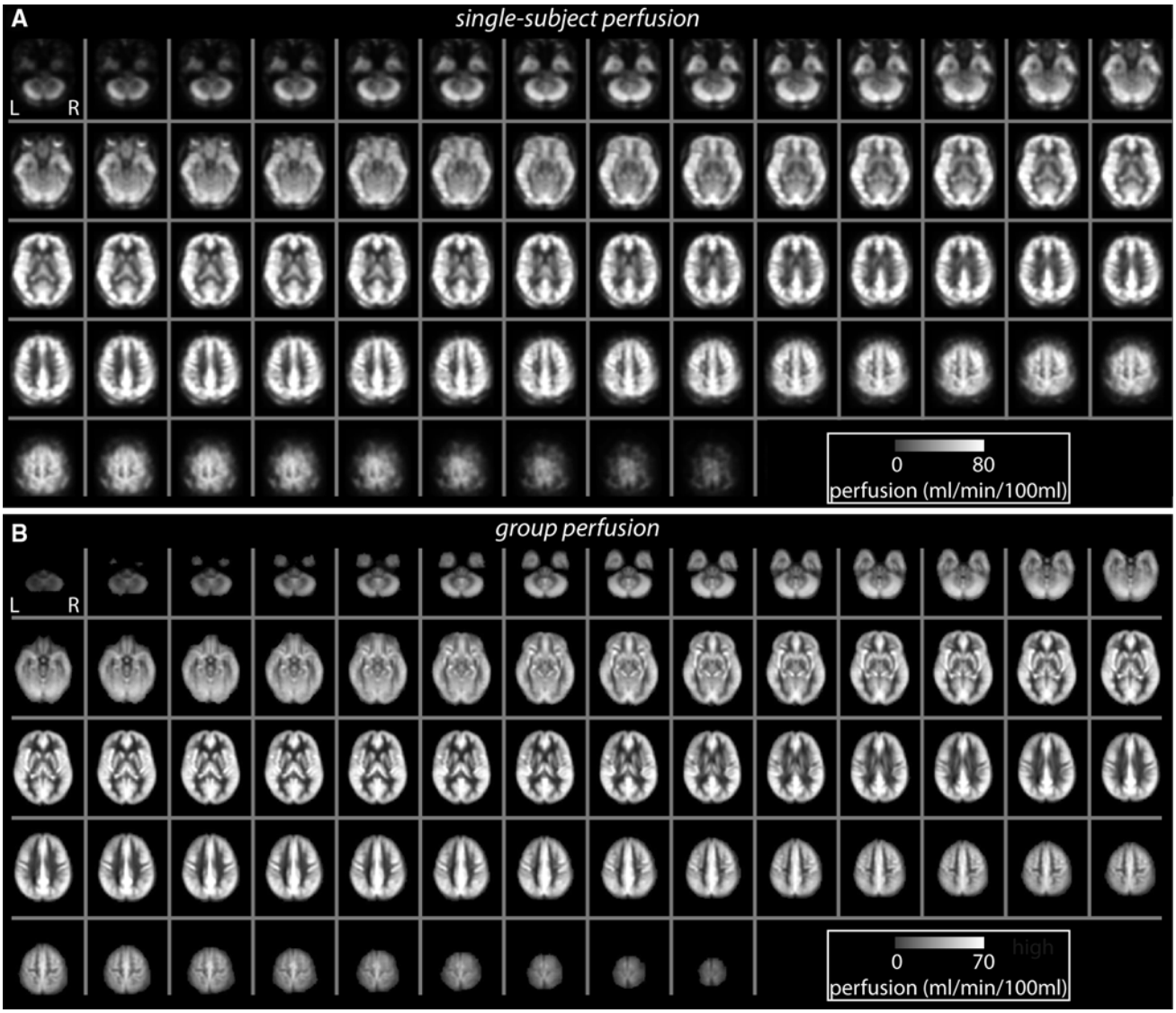

Fig. 4 Resting whole-brain perfusion. **a** Results for a single-subject and, **b** a group perfusion map generated from the average perfusion across all subjects

electric field, such that the postsynaptic neuronal activity (as opposed to axonal spiking) produces a signal detectable by EEG measurements (Speckman et al. 1993). In rats, a strong correlation has been observed in the cerebellar cortex between the product of field potential amplitude, stimulus frequency, and CBF (Mathiesen et al. 1998). In the visual cortex of the monkey, BOLD activation appears to be more closely linked to the neural activity related to the input and the local processing in any given area, rather than the spiking activity commonly thought of as the output of the area (Logothetis et al. 2001). Therefore, we suggest that the EEG signal and rCBF measurements might be based on the same neurophysiologic phenomenon (i.e., local postsynaptic activity), which is responsible for the strong correlation seen between both modalities.

An increase or decrease in measured BOLD fMRI signal in a local brain region compared to a baseline condition is usually interpreted as an increase (activation) or decrease (deactivation) in metabolism and local hemodynamic response. However, it has been proposed that the baseline (i.e., resting state) of cerebral metabolism reflects a state that yields a uniform oxygen extraction fraction throughout the brain (Gusnard et al. 2001; Raichle et al. 2001) and that any (de-)activation related to mental tasks or stimuli merely reflect relative changes from the baseline state. Recently, it has been shown that measures of electrophysiological (i.e., visual evoked potentials) and hemodynamic (BOLD and ASL) visual activity show the well-described steady habituation effect to repetitive stimulation (i.e., a decrease of amplitude) through the experiment, in which alternating blocks of contrast-reversing visual stimuli and blocks of rest (visual fixation) were presented (Mayhew et al. 2010). Although it is still unclear whether transient BOLD responses have vascular or a neuronal origin (Obata et al. 2004; Fox et al. 2005), we would argue these findings further underline the tight relationship between electrophysiological and hemodynamic measures not only during rest but also during stimulation.

EEG Power: ASL Effects

For the local EEG power—ASL correlations, the most striking finding was the variation in sign and spatial extent for different frequency bands. In this context, the positive Correlation between relative perfusion and alpha power indicate that subjects who have a higher resting alpha power show higher perfusion in brain regions than subjects with a lower resting alpha power. Although several simultaneous EEG-fMRI studies have shown negative correlations between alpha power and the BOLD signal during rest (Goldman et al. 2002; Laufs et al. 2003b, 2006; Moosmann et al. 2003; Feige et al. 2005; Goncalves et al. 2006; De Munck et al. 2007, 2008; Ben-Simon et al. 2008; Ritter et al. 2009), these findings may be consistent with our observation of mostly positive correlations between alpha power and resting perfusion if higher baseline resting perfusion is associated with a lower BOLD signal response during a task. This inverse relationship between baseline perfusion and the BOLD response has been reported previously (Goldman et al. 2002; Moosmann et al. 2003; Feige et al. 2005; De Munck et al. 2007; Tyvaert et al. 2008), and is supported by results from calibrated BOLD fMRI studies (Uludag et al. 2004; Shulman et al. 2007), but further simultaneous EEG-ASL-BOLD studies would be necessary to establish whether the higher perfusion seen in subjects with high alpha power in this study engenders a higher task-evoked hemodynamic response or a smaller change relative to baseline. In contrast to alpha, it has been noted that gamma-BOLD signal correlations are predominately positive during rest, visual stimulation and working memory, as shown by EEG-fMRI and electrophysiological studies in human adults (Laufs et al. 2003b; Niessing et al. 2005; Nir et al. 2007; Michels et al. 2010). A recent electrophysiological study in humans found a positive coupling between gamma LFP and the BOLD signal (Nir et al. 2007; Logothetis et al. 2001). Interestingly, the coupling was high ($r \geq 0.62$) when the interneuronal-firing-rate was high, indicating that the examined between-modality correlations are tightly related to the degree of interneuronal correlations. Therefore, the observed positive correlations between gamma band power and whole-brain perfusion may arise from high interneuronal correlations. However, since it is not entirely clear what conditions may create high or low correlations among neurons, and since variability in interneuronal correlation can be found for stimulation and rest conditions (Nir et al. 2007), spike-gamma or spike-BOLD correlations can be used as an index for the level of correlated firing-rate modulation in the cortex. Further research will therefore be necessary to investigate whether spike-ASL or gamma-ASL correlations are coupled to interneuronal correlations. The observed finding of positive beta-ASL and gamma-ASL correlations is also consistent with a previous FDG-PET study, which reported an increase in the number of positively correlated voxels with increasing EEG frequency (Oakes et al. 2004).

A general observation was that the alpha and gamma as well as theta and beta EEG-ASL correlations appear rather similar, and thus follow the conventional frequency band groupings (slow–fast) also evident in EEG-power BOLD signal coupling findings (Lüchinger et al. 2012). This overlap may provide evidence for the theory of nested frequencies recently proposed to underlie working memory (Lisman 2010). However, it differs from the prominent cross-frequency theta-gamma coupling observed by others (Jensen and Colgin 2007), and should be explored in future intracranial or EEG/MEG source localization studies.

Local Versus Global EEG Power

Global EEG power, i.e., the total power over the whole scalp, does not fully capture locally specific brain rhythms (e.g., visual alpha). Hence, we performed a subsequent correlation analysis in which we selected the alpha EEG power values for a single occipital electrode and from right or left hemispheric scalp electrodes (Fig. 2), since topographical maps (Fig. 3), indicated that EEG power was enhanced at this electrode not only in alpha but also in other frequency bands. However, the sign of the correlation and the overall spatial pattern remained the same or similar to that seen for the global EEG-ASL correlation analysis (Fig. 2). Interestingly, resting- and task-related EEG-fMRI studies have also demonstrated a strong similarity in the correlation pattern between the BOLD signal and whole-scalp (i.e., RMS) EEG power and between the BOLD signal and spatially-restricted EEG power (Scheeringa et al. 2009; Michels et al. 2010; Lüchinger et al. 2011). In the study by Larson et al. (1998) alpha power was quantified in a single measure, as it was derived from all electrode contacts. Thus, we argue that the RMS approach may reflect locally dominant brain rhythms, such as the parieto-occipital (visual) alpha rhythm.

EEG Central Frequency: ASL Effects

Further, we demonstrated that alpha central frequency, a neurobiological correlate of an individual's cognitive resources (Klimesch 1999; Klimesch et al. 1999), was positively linked to perfusion in various brain regions which are engaged in task-execution, such as the post-central and inferior frontal gyrus. Thus we could replicate the findings from a recent EEG-ASL study (Jann et al. 2010) and from a previous EEG-PET study (Alper et al. 2006), since these studies reported predominantly or exclusively positive correlations between alpha frequency and regional perfusion in similar regions. Additionally, we have shown for the first time that central theta frequency is negatively correlated to perfusion in a widespread network of cortical brain regions. The underlying cause of this correlation is unclear, although the coupling between theta frequency and perfusion may be sensitive to age, gender, and IQ effects. Since the participant group consisted of young healthy adults and age and gender were included as covariates in the statistical analysis, it seems unlikely that this result arises purely from to age- or gender-related perfusion and EEG changes. However, alterations in peak delta, theta, and alpha frequency (and perfusion) have been reported in the context of traumatic brain injury (Fedor et al. 2010; Kim et al. 2012) schizophrenia (Koukkou et al. 2000), and chronic pain (Sarnthein et al. 2006; Bakhtadze et al. 2012), and related to cognitive or memory impairments (Kim et al. 2012) as well as immaturity (Koukkou et al. 2000). Therefore, the link between theta central frequency and perfusion may reflect individual differences in cognitive abilities or IQ or other factors such as the level of excitability of neuronal networks (Koukkou et al. 2000), but further investigations including task-related studies will be necessary to elucidate the underlying cause of this apparent theta central frequency ASL interaction. Recently, it has been shown that gamma peak frequency is negatively correlated to the BOLD signal during visual stimulation (Muthukumaraswamy et al. 2009). Here we observed modest but exclusively negative correlations between central gamma frequency and perfusion in inferior frontal, temporal, and parietal regions, which may thus reflect a general association between gamma frequency and cerebral haemodynamics.

Interaction Between Central Frequency and Power

There is evidence that EEG frequency and power are interrelated measures (Klimesch 1999), when it comes to capturing spectral shifts from slower to faster frequencies occurring with maturation (Lüchinger et al. 2011, 2012), increasing vigilance or activation within and across frequency bands.(Buzsaki 2006). On the other hand, power in certain specific frequency bands and regions has also been related to more specific cognitive functions. For example, it has been shown recently that visual stimulation leads to an increase in gamma power and BOLD amplitude. At the same time, BOLD amplitude (and most likely gamma power) was inversely related to peak frequency (Muthukumaraswamy et al. 2009). Thus, at least for stimulation paradigms it can be assumed that high-frequency power and (central) peak frequency are correlated measures. In various clinical populations (e.g., chronic pain, Parkinson's disease, epilepsy) it is known that power is enhanced compared to healthy controls while in parallel peak frequency is shifted towards lower alpha and upper theta band (e.g., Sarnthein et al. 2006), suggesting an inverse relation between power and frequency. In contrast, in patients with vascular dementia lower alpha power was linked to a slowing in alpha frequency (Moretti et al. 2004), suggesting that the coupling between resting power and central frequency may be disrupted by specific disease processes. Such inverse relations would predict opposite signs of the CBF correlation maps with power and central frequency, respectively. This pattern was indeed observed for delta, theta and gamma, but the results for alpha and beta are inconsistent with the assumption of a strong inverse relation. Our correlation results thus indicate that both power and frequency appear to be associated with perfusion, although the directional and regional involvement differs for power and central frequency. This suggests that while

both EEG power and frequency are most probably linked to perfusion via fundamental metabolic processes, EEG power and central frequency provide a complementary rather than overlapping insight into the link between baseline EEG oscillations and haemodynamics.

Limitations

Nonuniformity in the perfusion images could present a potential confound for the EEG-ASL effects, as the signal-to-noise ratio (SNR) of the perfusion data may limit the sensitivity to EEG correlations in certain brain regions. However, the PCASL method used in this study offers high perfusion SNR relative to alternative labelling schemes (Wu et al. 2007), and the 3D stack of spirals readout does not suffer from dropout in temporal or orbitofrontal brain regions, offering improved uniformity relative to EPI (Dai et al. 2008; Järnum et al. 2010). The perfusion images therefore demonstrate high SNR and uniformity across the whole brain (see Fig. 4 for a single subject and group average perfusion map), so the uniformity of the perfusion images does not appear to be the limiting factor governing the sensitivity of the EEG-ASL correlations.

Another potential confound could arise from changes in brain state between the ASL and EEG measurements, since the measurements were not performed simultaneously. However, while both the EEG and local perfusion demonstrate transient state-dependent changes during stimulation or a behavioural task, both the resting perfusion and baseline EEG power and alpha mean frequency show high reliability, both within- and between-session. The within-session reproducibility for grey matter perfusion has been estimated at 5 % using PCASL during an uncontrolled resting state, and remain stable even over time intervals of days or weeks (Wang et al. 2003; Parkes et al. 2004; O'Gorman et al. 2007).

In a similar manner as for perfusion, the EEG can also be considered a trait marker, as it is known that absolute resting alpha power and the shape of the spectral curve show very low test–retest variability in healthy adults, even if two consecutive recordings are performed with a gap of several months (e.g., Näpflin et al. 2007). As pointed out by several studies, it is advisable to use absolute power (as used in this study) rather than relative power for analysis (Pollack 1991; Kondacs and Szabó 1999). In general, retest reliability of spectral resting EEG band power in adults is high for all classical EEG frequency bands (Stassen 1980; Salinsky et al. 1991; Dustman et al. 1999; Kondacs and Szabó 1999; Poulos et al. 2002; Maltez et al. 2004), averaging more than 0.8 over several months, and even exceeding 0.9 over a few minutes (Salinsky et al. 1991). Thus, it seems unlikely that the correlation results are confounded by state-dependent differences between the (consecutive) EEG and ASL recordings.

Conclusions

This study has revealed a coupling between perfusion and EEG power and central frequency across all frequency bands, and a variation in the direction and the neuronal substrate of EEG-ASL coupling for different frequencies. We conclude that brain haemodynamics are coupled to brain oscillations at the level of absolute fluctuations in electromagnetic activity, and that cerebral blood flow is differentially linked to low and high frequency brain oscillations.

Acknowledgments This work was supported by the NCCR on Neural Plasticity and Repair, and by the University Research Priority Program on Integrative Human Physiology. We thank Dr. John Suckling and the developer teams at Cambridge University and the Institute of Psychiatry, King's College London (London, UK) for advice regarding the CamBA installation and analysis.

References

Aguirre GK, Detre JA, Zarahn E, Alsop DC (2002) Experimental design and the relative sensitivity of BOLD and perfusion fMRI. Neuroimage 15:488–500

Alkire MT (2008) Probing the mind: anesthesia and neuroimaging. Clin Pharmacol Ther 84:149–152

Almeida R, Stetter M (2002) Modeling the link between functional imaging and neuronal activity: synaptic metabolic demand and spike rates. Neuroimage 17:1065–1079

Alper KR, John ER, Brodie J, Günther W, Daruwala R, Prichep LS (2006) Correlation of PET and qEEG in normal subjects. Psychiatry Res 146:271–282

Alsop DC, Detre JA (1996) Reduced transit-time sensitivity in noninvasive magnetic resonance imaging of human cerebral blood flow. J Cereb Blood Flow Metab 16:1236–1249

Axmacher N, Mormann F, Fernández G, Elger CE, Fell J (2006) Memory formation by neuronal synchronization. Brain Res Rev 52:170–182

Bakhtadze MA, Vernon H, Karalkin AV, Pasha SP, Tomashevskiy IO, Soave D (2012) Cerebral perfusion in patients with chronic neck and upper back pain: preliminary observations. J Manipulative Physiol Ther 35:76–85

Bartlett EJ, Brodie JD, Wolf AP, Christman DR, Laska E, Meissner M (1988) Reproducibility of cerebral glucose metabolic measurements in resting human subjects. J Cereb Blood Flow Metab 8:502–512

Ben-Simon E, Podlipsky I, Arieli A, Zhdanov A, Hendler T (2008) Never resting brain: simultaneous representation of two alpha related processes in humans. PLoS One 3:e3984

Binder JR, Frost JA, Hammeke TA, Bellgowan PSF, Rao SM, Cox RW (1999) Conceptual processing during the conscious resting state: a functional MRI study. J Cogn Neurosci 11:80–93

Brem S, Bach S, Kucian K, Guttorm TK, Martin E, Lyytinen H, Brandeis D, Richardson U (2010) Brain sensitivity to print

emerges when children learn letter-speech sound correspondences. Proc Natl Acad Sci USA 107:7939
Brown GG, Perthen JE, Liu TT, Buxton RB (2007) A primer on functional magnetic resonance imaging. Neuropsychol Rev 17:107–125
Buckner RL (2004) Memory and executive function in aging and AD: multiple factors that cause decline and reserve factors that compensate. Neuron 44:195–208
Buxton RB, Uludag K, Dubowitz DJ, Liu TT (2004) Modeling the hemodynamic response to brain activation. Neuroimage 23:S220–S233
Buzsaki G (2006) Rhythms of the brain. Oxford University Press, Oxford
Chamberlain SR, Hampshire A, Müller U, Rubia K, Del Campo N, Craig K, Regenthal R, Suckling J, Roiser JP, Grant JE et al (2009) Atomoxetine modulates right inferior frontal activation during inhibitory control: a pharmacological functional magnetic resonance imaging study. Biol Psychiatry 65:550–555
Dai W, Garcia D, De Bazelaire C, Alsop DC (2008) Continuous flow-driven inversion for arterial spin labeling using pulsed radio frequency and gradient fields. Magn Reson Med 60:1488–1497
Danos P, Guich S, Abel L, Buchsbaum MS (2001) EEG alpha rhythm and glucose metabolic rate in the thalamus in schizophrenia. Neuropsychobiology 43:265–272
De Lange FP, Jensen O, Bauer M, Toni I (2008) Interactions between posterior gamma and frontal alpha/beta oscillations during imagined actions. Front Hum Neurosci 2:7
De Munck JC, Goncalves SI, Huijboom L, Kuijer JPA, Pouwels PJW, Heethaar RM, Lopes da Silva FH (2007) The hemodynamic response of the alpha rhythm: an EEG/fMRI study. Neuroimage 35:1142–1151
De Munck JC, Goncalves SI, Faes TJC, Kuijer JPA, Pouwels PJW, Heethaar RM, Lopes da Silva FH (2008) A study of the brain's resting state based on alpha band power, heart rate and fMRI. Neuroimage 42:112–121
Delorme A, Makeig S (2004) EEGLAB: an open source toolbox for analysis of single-trial EEG dynamics including independent component analysis. J Neurosci Methods 134:9–21
Dierks T, Jelic V, Pascual-Marqui RD, Wahlund LO, Julin P, Linden DEJ, Maurer K, Winblad B, Nordberg A (2000) Spatial pattern of cerebral glucose metabolism (PET) correlates with localization of intracerebral EEG-generators in Alzheimer's disease. Clin Neurophysiol 111:1817–1824
Duong TQ, Kim DS, Uğurbil K, Kim SG (2001) Localized cerebral blood flow response at submillimeter columnar resolution. Proc Natl Acad Sci USA 98:10904
Dustman RE, Shearer DE, Emmerson RY (1999) Life-span changes in EEG spectral amplitude, amplitude variability and mean frequency. Clin Neurophysiol 110:1399–1409
Eichele T, Specht K, Moosmann M, Jongsma MLA, Quiroga RQ, Nordby H, Hugdahl K (2005) Assessing the spatiotemporal evolution of neuronal activation with single-trial event-related potentials and functional MRI. Proc Natl Acad Sci USA 102:17798
Fedor M, Berman RF, Muizelaar JP, Lyeth BG (2010) Hippocampal theta dysfunction after lateral fluid percussion injury. J Neurotrauma 27:1605–1615
Feige B, Scheffler K, Esposito F, Di Salle F, Hennig J, Seifritz E (2005) Cortical and subcortical correlates of electroencephalographic alpha rhythm modulation. J Neurophysiol 93:2864–2872
Fox MD, Raichle ME (2007) Spontaneous fluctuations in brain activity observed with functional magnetic resonance imaging. Nat Rev Neurosci 8:700–711
Fox MD, Snyder AZ, McAvoy MP, Barch DM, Raichle ME (2005) The BOLD onset transient: identification of novel functional differences in schizophrenia. Neuroimage 25:771–782
Goldman RI, Stern JM, Engel J Jr, Cohen MS (2002) Simultaneous EEG and fMRI of the alpha rhythm. Neuroreport 13:2487
Goncalves SI, De Munck JC, Pouwels PJW, Schoonhoven R, Kuijer JPA, Maurits NM, Hoogduin JM, Van Someren EJW, Heethaar RM, Lopes da Silva FH (2006) Correlating the alpha rhythm to BOLD using simultaneous EEG/fMRI: inter-subject variability. Neuroimage 30:203–213
Gruber T, Keil A, Müller MM (2001) Modulation of induced gamma band responses and phase synchrony in a paired associate learning task in the human EEG. Neurosci Lett 316: 29–32
Gusnard DA, Raichle ME, Raichle ME et al (2001) Searching for a baseline: functional imaging and the resting human brain. Nat Rev Neurosci 2:685–694
Halder P, Sterr A, Brem S, Bucher K, Kollias S, Brandeis D (2005) Electrophysiological evidence for cortical plasticity with movement repetition. Eur J Neurosci 21:2271–2277
Hoge RD, Pike GB (2001) Oxidative metabolism and the detection of neuronal activation via imaging. J Chem Neuroanat 22:43–52
Ingvar DH, Sjölund B, Ardö A (1976) Correlation between dominant EEG frequency, cerebral oxygen uptake and blood flow. Electroencephalogr Clin Neurophysiol 41:268–276
Ingvar DH, Rosén I, Johannesson G (1979) EEG related to cerebral metabolism and blood flow. Pharmacopsychiatry 12:200–209
Jahng GH, Song E, Zhu XP, Matson GB, Weiner MW, Schuff N (2005) Human brain: reliability and reproducibility of pulsed arterial spin-labeling perfusion MR imaging1. Radiology 234:909–916
Jann K, Dierks T, Boesch C, Kottlow M, Strik W, Koenig T (2009) BOLD correlates of EEG alpha phase-locking and the fMRI default mode network. Neuroimage 45:903–916
Jann K, Koenig T, Dierks T, Boesch C, Federspiel A (2010) Association of individual resting state EEG alpha frequency and cerebral blood flow. Neuroimage 51:365–372
Järnum H, Steffensen EG, Knutsson L, Fründ ET, Simonsen CW, Lundbye-Christensen S, Shankaranarayanan A, Alsop DC, Jensen FT, Larsson EM (2010) Perfusion MRI of brain tumours: a comparative study of pseudo-continuous arterial spin labelling and dynamic susceptibility contrast imaging. Neuroradiology 52:307–317
Jelic V, König T, Dierks T, Nordberg A, Wahlund L-O (2002) Electroencephalography and glucose metabolism (positron-emission tomography) in dementing disorders. Methods Find Exp Clin Pharmacol 24:21
Jensen O, Colgin LL (2007) Cross-frequency coupling between neuronal oscillations. Trends Cogn Sci 11:267–269
Jensen O, Gelfand J, Kounios J, Lisman JE (2002) Oscillations in the alpha band (9–12 Hz) increase with memory load during retention in a short-term memory task. Cereb Cortex 12:877–882
Jokisch D, Jensen O (2007) Modulation of gamma and alpha activity during a working memory task engaging the dorsal or ventral stream. J Neurosci 27:3244–3251
Jung TP, Makeig S, Humphries C, Lee TW, Mckeown MJ, Iragui V, Sejnowski TJ (2000a) Removing electroencephalographic artifacts by blind source separation. Psychophysiology 37:163–178
Jung TP, Makeig S, Westerfield M, Townsend J, Courchesne E, Sejnowski TJ (2000b) Removal of eye activity artifacts from visual event-related potentials in normal and clinical subjects. Clin Neurophysiol 111:1745–1758
Kida I, Hyder F et al (2006) Physiology of functional magnetic resonance imaging: energetics and function. Methods Mol Med 124:175
Kim J, Whyte J, Patel S, Europa E, Slattery J, Coslett HB, Detre JA (2012) A perfusion fMRI study of the neural correlates of sustained-attention and working-memory deficits in chronic traumatic brain injury. Neurorehabil Neural Repair 26:870–880

Klimesch W (1999) EEG alpha and theta oscillations reflect cognitive and memory performance: a review and analysis. Brain Res Rev 29(2–3):169–195

Klimesch et al (1999) Interindividual differences in alpha and theta power reflect memory performance. Intelligence 27(4):347–362

Kondacs A, Szabó M (1999) Long-term intra-individual variability of the background EEG in normals. Clin Neurophysiol 110:1708–1716

Koukkou M, Federspiel A, Bräker E, Hug C, Kleinlogel H, Merlo MCG, Lehmann D (2000) An EEG approach to the neurodevelopmental hypothesis of schizophrenia studying schizophrenics, normal controls and adolescents. J Psychiatr Res 34:57–73

Kranczioch C, Debener S, Herrmann CS, Engel AK (2006) EEG gamma-band activity in rapid serial visual presentation. Exp Brain Res 169:246–254

Kuhl BA, Dudukovic NM, Kahn I, Wagner AD (2007) Decreased demands on cognitive control reveal the neural processing benefits of forgetting. Nat Neurosci 10:908–914

Kuschinsky W, Bünger R, Schröck H, Mallet RT, Sokoloff L (1993) Local glucose utilization and local blood flow in hearts of awake rats. Basic Res Cardiol 88:233–249

Larson CL, Davidson RJ, Abercrombie HC, Ward RT, Schaefer SM, Jackson DC, Holden JE, Perlman SB (1998) Relations between PET-derived measures of thalamic glucose metabolism and EEG alpha power. Psychophysiology 35:162–169

Laufs H, Kleinschmidt A, Beyerle A, Eger E, Salek-Haddadi A, Preibisch C, Krakow K (2003a) EEG-correlated fMRI of human alpha activity. Neuroimage 19:1463–1476

Laufs H, Krakow K, Sterzer P, Eger E, Beyerle A, Salek-Haddadi A, Kleinschmidt A (2003b) Electroencephalographic signatures of attentional and cognitive default modes in spontaneous brain activity fluctuations at rest. Proc Natl Acad Sci USA 100:11053

Laufs H, Holt JL, Elfont R, Krams M, Paul JS, Krakow K, Kleinschmidt A (2006) Where the BOLD signal goes when alpha EEG leaves. Neuroimage 31:1408–1418

Lehmann D, Skrandies W (1980) Reference-free identification of components of checkerboard-evoked multichannel potential fields. Electroencephalogr Clin Neurophysiol 48:609–621

Lindgren KA, Larson CL, Schaefer SM, Abercrombie HC, Ward RT, Oakes TR, Holden JE, Perlman SB, Benca RM, Davidson RJ (1999) Thalamic metabolic rate predicts EEG alpha power in healthy control subjects but not in depressed patients. Biol Psychiatry 45:943–952

Lisman J (2010) Working memory: the importance of theta and gamma oscillations. Curr Biol 20(11):R490–R492

Liu X, Zhu XH, Zhang Y, Chen W (2011) Neural origin of spontaneous hemodynamic fluctuations in rats under burst-suppression anesthesia condition. Cereb Cortex 21:374–384

Logothetis NK, Pauls J, Augath M, Trinath T, Oeltermann A et al (2001) Neurophysiological investigation of the basis of the fMRI signal. Nature 412:150–157

Lüchinger R, Michels L, Martin E, Brandeis D (2011) EEG-BOLD correlations during (post-) adolescent brain maturation. Neuroimage 56:1493–1505

Lüchinger R, Michels L, Martin E, Brandeis D (2012) Brain state regulation during normal development: intrinsic activity fluctuations in simultaneous EEG-fMRI. Neuroimage 60:1426–1439

Maltez J, Hyllienmark L, Nikulin VV, Brismar T (2004) Time course and variability of power in different frequency bands of EEG during resting conditions. Neurophysiol Clin 34:195–202

Mathiesen C, Caesar K, Akgören N, Lauritzen M (1998) Modification of activity-dependent increases of cerebral blood flow by excitatory synaptic activity and spikes in rat cerebellar cortex. J F Physiol 512:555–566

Maurer U, Brem S, Bucher K, Kranz F, Benz R, Steinhausen HC, Brandeis D (2007) Impaired tuning of a fast occipito-temporal response for print in dyslexic children learning to read. Brain 130:3200–3210

Mayhew SD, Macintosh BJ, Dirckx SG, Iannetti GD, Wise RG (2010) Coupling of simultaneously acquired electrophysiological and haemodynamic responses during visual stimulation. Magn Reson Imaging 28:1066–1077

Meltzer JA, Negishi M, Mayes LC, Constable RT (2007) Individual differences in EEG theta and alpha dynamics during working memory correlate with fMRI responses across subjects. Clin Neurophysiol 118:2419–2436

Meltzer JA, Fonzo GA, Constable RT (2009) Transverse patterning dissociates human EEG theta power and hippocampal BOLD activation. Psychophysiology 46:153–162

Michels L, Bucher K, Lüchinger R, Klaver P, Martin E, Jeanmonod D, Brandeis D (2010) Simultaneous EEG-fMRI during a working memory task: modulations in low and high frequency bands. PLoS One 5:e10298

Michels L, Luchinger R, Koenig T, Martin E, Brandeis D (2012) Developmental changes of BOLD signal correlations with global human EEG power and synchronization during working memory. PLoS One 7:e39447

Montez T, Poil SS, Jones BF, Manshanden I, Verbunt J, Van Dijk BW, Brussaard AB, Van Ooyen A, Stam CJ, Scheltens P et al (2009) Altered temporal correlations in parietal alpha and prefrontal theta oscillations in early-stage Alzheimer disease. Proc Natl Acad Sci USA 106:1614

Moosmann M, Ritter P, Krastel I, Brink A, Thees S, Blankenburg F, Taskin B, Obrig H, Villringer A (2003) Correlates of alpha rhythm in functional magnetic resonance imaging and near infrared spectroscopy. Neuroimage 20:145–158

Moretti DV, Babiloni C, Binetti G, Cassetta E, Dal Forno G, Ferreric F, Ferri R, Lanuzza B, Miniussi C, Nobili F et al (2004) Individual analysis of EEG frequency and band power in mild Alzheimer's disease. Clin Neurophysiol 115:299–308

Muthukumaraswamy SD, Edden RAE, Jones DK, Swettenham JB, Singh KD (2009) Resting GABA concentration predicts peak gamma frequency and fMRI amplitude in response to visual stimulation in humans. Proc Natl Acad Sci USA 106:8356

Nagata K (1988) Topographic EEG in brain ischemia-Correlation with blood flow and metabolism. Brain Topogr 1:97–106

Näpflin M, Wildi M, Sarnthein J (2007) Test–retest reliability of resting EEG spectra validates a statistical signature of persons. Clin Neurophysiol 118:2519–2524

Niedermeyer E, Silva FHLD (2005) Electroencephalography: basic Principles, clinical applications, and related fields. Lippincott Williams & Wilkins, Philadelphia

Niessing J, Ebisch B, Schmidt KE, Niessing M, Singer W, Galuske RAW (2005) Hemodynamic signals correlate tightly with synchronized gamma oscillations. Science 309:948–951

Nir Y, Fisch L, Mukamel R, Gelbard-Sagiv H, Arieli A, Fried I, Malach R (2007) Coupling between neuronal firing rate, gamma LFP, and BOLD fMRI is related to interneuronal correlations. Curr Biol 17:1275–1285

O'Gorman R, Coward H, Zelaya F, Alsop DC, Williams SCR (2007) Reproducibility of pseudo-continuous ASL at 1.5T and 3T. ISMRM 15:1419

Oakes TR, Pizzagalli DA, Hendrick AM, Horras KA, Larson CL, Abercrombie HC, Schaefer SM, Koger JV, Davidson RJ (2004) Functional coupling of simultaneous electrical and metabolic activity in the human brain. Hum Brain Mapp 21:257–270

Obata T, Liu TT, Miller KL, Luh WM, Wong EC, Frank LR, Buxton RB (2004) Discrepancies between BOLD and flow dynamics in primary and supplementary motor areas: application of the balloon model to the interpretation of BOLD transients. Neuroimage 21:144–153

Ogawa S, Menon RS, Tank DW, Kim SG, Merkle H, Ellermann JM, Ugurbil K (1993) Functional brain mapping by blood oxygenation level-dependent contrast magnetic resonance imaging. A comparison of signal characteristics with a biophysical model. Biophys J 64:803–812

Parkes LM, Rashid W, Chard DT, Tofts PS (2004) Normal cerebral perfusion measurements using arterial spin labeling: reproducibility, stability, and age and gender effects. Magn Reson Med 51:736–743

Pilgreen KL (1995) Physiologic, medical, and cognitive correlates of electroencephalography. Neocortical dynamics and human EEG rhythms. Oxford University Press, New York, pp 195–248

Pollack JB (1991) The induction of dynamical recognizers. Mach Learn 7:227–252

Poulos M, Rangoussi M, Alexandris N, Evangelou A (2002) Person identification from the EEG using nonlinear signal classification. Methods Inf Med 41:64–75

Raghavachari S, Kahana MJ, Rizzuto DS, Caplan JB, Kirschen MP, Bourgeois B, Madsen JR, Lisman JE (2001) Gating of human theta oscillations by a working memory task. J Neurosci 21:3175–3183

Raichle ME, MacLeod AM, Snyder AZ, Powers WJ, Gusnard DA, Shulman GL (2001) A default mode of brain function. Proc Natl Acad Sci USA 98:676

Ritter P, Moosmann M, Villringer A (2009) Rolandic alpha and beta EEG rhythms' strengths are inversely related to fMRI-BOLD signal in primary somatosensory and motor cortex. Hum Brain Mapp 30:1168–1187

Sadato N, Nakamura S, Oohashi T, Nishina E, Fuwamoto Y, Waki A, Yonekura Y (1998) Neural networks for generation and suppression of alpha rhythm: a PET study. Neuroreport 9:893

Salinsky MC, Oken BS, Morehead L (1991) Test–retest reliability in EEG frequency analysis. Electroencephalogr Clin Neurophysiol 79:382–392

Sammer G, Blecker C, Gebhardt H, Bischoff M, Stark R, Morgen K, Vaitl D (2007) Relationship between regional hemodynamic activity and simultaneously recorded EEG-theta associated with mental arithmetic-induced workload. Hum Brain Mapp 28:793–803

Sarnthein J, Stern J, Aufenberg C, Rousson V, Jeanmonod D (2006) Increased EEG power and slowed dominant frequency in patients with neurogenic pain. Brain 129:55–64

Scheeringa R, Petersson KM, Oostenveld R, Norris DG, Hagoort P, Bastiaansen M (2009) Trial-by-trial coupling between EEG and BOLD identifies networks related to alpha and theta EEG power increases during working memory maintenance. Neuroimage 44:1224–1238

Scheeringa R, Fries P, Petersson KM, Oostenveld R, Grothe I, Norris DG, Hagoort P, Bastiaansen M (2011) Neuronal dynamics underlying high-and low-frequency EEG oscillations contribute independently to the human BOLD signal. Neuron 69:572–583

Shulman RG, Rothman DL, Hyder F (2007) A BOLD search for baseline. Neuroimage 36:277–281

Speckman EJ, Elger CE, Altrup U (1993) Neurophysiologic basis of the EEG. The treatment of epilepsy: principles and practices. Lea and Febiger, Philadelphia

Stassen HH (1980) Computerized recognition of persons by EEG spectral patterns. Electroencephalogr Clin Neurophysiol 49:190–194

Suckling J, Bullmore E (2004) Permutation tests for factorially designed neuroimaging experiments. Hum Brain Mapp 22:193–205

Talairach J, Tournoux P (1988) Co-planar stereotaxic atlas of the human brain: 3-dimensional proportional system: an approach to cerebral imaging. Thieme, Stuttgart

Tjandra T, Brooks JCW, Figueiredo P, Wise R, Matthews PM, Tracey I (2005) Quantitative assessment of the reproducibility of functional activation measured with BOLD and MR perfusion imaging: implications for clinical trial design. Neuroimage 27:393–401

Tuladhar AM, Huurne N, Schoffelen JM, Maris E, Oostenveld R, Jensen O (2007) Parieto-occipital sources account for the increase in alpha activity with working memory load. Hum Brain Mapp 28:785–792

Tyvaert L, LeVan P, Grova C, Dubeau F, Gotman J (2008) Effects of fluctuating physiological rhythms during prolonged EEG-fMRI studies. Clin Neurophysiol 119:2762–2774

Uludag K, Dubowitz DJ, Yoder EJ, Restom K, Liu TT, Buxton RB (2004) Coupling of cerebral blood flow and oxygen consumption during physiological activation and deactivation measured with fMRI. Neuroimage 23:148–155

Van der Werf J, Jensen O, Fries P, Medendorp WP (2008) Gamma-band activity in human posterior parietal cortex encodes the motor goal during delayed prosaccades and antisaccades. J Neurosci 28:8397–8405

Vural C, Yildiz M (2010) Determination of sleep stage separation ability of features extracted from EEG signals using principle component analysis. J Med Syst 34:83–89

Wang J, Aguirre GK, Kimberg DY, Roc AC, Li L, Detre JA (2003) Arterial spin labeling perfusion fMRI with very low task frequency. Magn Reson Med 49:796–802

Wang J, Zhang Y, Wolf RL, Roc AC, Alsop DC, Detre JA (2005) Amplitude-modulated continuous arterial spin-labeling 3.0-T perfusion MR imaging with a single coil: feasibility study1. Radiology 235:218–228

Wastling SJ, O'Daly O, Zelaya O, Howard M, Alsop DC, O'Gorman RL (2009) Quantitative comparison of methods for spatial normalisation of CASL perfusion MR images. ISMRM 17:2909

Wu WC, Fernández-Seara M, Detre JA, Wehrli FW, Wang J (2007) A theoretical and experimental investigation of the tagging efficiency of pseudocontinuous arterial spin labeling. Magn Reson Med 58:1020–1027